Submitted to the Annals of Applied Statistics

INFERENCE FOR DEFORMATION AND INTERFERENCE IN 3D PRINTING

By Arman Sabbaghi*, Tirthankar Dasgupta†, Qiang Huang‡, and Jizhe Zhang

Harvard University, Harvard University, University of Southern California, and University of Southern California

Additive manufacturing, or 3D printing, is a promising manufacturing technique marred by product deformation due to material solidification in the printing process. Control of printed product deformation can be achieved by a compensation plan. However, little attention has been paid to interference in compensation, which is thought to result from the inevitable discretization of a compensation plan. We investigate interference with an experiment involving the application of discretized compensation plans to cylinders. Our treatment illustrates a principled framework for detecting and modeling interference that facilitates the study of printed product deformation under discretized compensation plans. Properly defining experimental units and understanding interference are critical for quality control in complex manufacturing processes. Our work provides a step in that direction for 3D printing.

1. Interference in Compensation. Additive manufacturing, or 3D printing, refers to a class of technology for the direct fabrication of physical products from 3D Computer-Aided Design (CAD) models. In contrast to material removal processes in traditional machining, the printing process adds material layer by layer. This enables direct printing of geometrically complex products without affecting building efficiency. No extra effort is necessary for molding construction or fixture tooling design, making 3D printing a promising manufacturing technique (Hilton and Jacobs, 2000; Gibson, Rosen, and Stucker, 2009; Melchels, Feijen, and Grijpma, 2010; Campbell, Williams, Ivanova, and Garrett, 2011). Despite these promising features, control of a product's printed dimensions (i.e., dimensional accuracy control) remains a major bottleneck. Material solidification during layer formation leads to product deformation, or shrinkage (Wang, Cheah, Fuh, and

*Research supported by National Science Foundation DGE-1144152.
†Research supported by National Science Foundation DMS-1107004.
‡Research supported by Office of Naval Research N000141110671.
AMS 2000 subject classifications: Primary 62P30; secondary 62K99
Keywords and phrases: additive manufacturing, posterior predictive checks, quality control, Rubin Causal Model, Stable Unit-Treatment Value Assumption.

Lu, 1996), which reduces the utility of printed products. Shrinkage control is crucial to overcome the accuracy barrier in 3D printing.

To control detailed features along the boundary of a printed product, Tong, Lehtihet, and Joshi (2003) and Tong et al. (2008) used polynomial regression models to first analyze shrinkage in different directions separately, and then compensate for product deformation by changing the original CAD accordingly. Unfortunately, their predictions are independent of the product's geometry, which is not consistent with the physical manufacturing process. Huang, Zhang, Sabbaghi, and Dasgupta (2013) built on this work, using polar coordinates to develop a physically consistent approach to model and compensate for shrinkage. Validation experiments suggest that this approach can achieve greater accuracy control.

An important issue not yet addressed is how the application of compensation to one section of a product will affect the deformation of neighboring sections. Compensation plans are always discretized according to the tolerance of the 3D printer, in the sense that sections of the CAD are altered by single amounts, e.g., as in Figure 1. Furthermore, when planning an experiment to assess the effect of compensations on product deformation, it is natural to discretize the quantitative "compensation" factor into a finite number of levels, which also leads to a product having a more complex boundary. Ultimately, such changes may introduce interference between different sections of the printed product, which is defined to occur when one section's deformation depends not only on its assigned compensation, but also on compensations applied to its neighbors (Rubin, 1980). For example, in Figure 1, the deformation for points near the boundary of two neighboring sections should depend on compensations applied to both sections. By the same logic, interference becomes a practical issue when printing products with complex geometry. Therefore, to improve dimensional accuracy control in 3D printing, it is important to formally investigate complications introduced by the interference that results from the inevitable discretization in compensation plans. We take the first step with an experiment involving a discretized compensation plan for a simple geometric shape.

We begin in Section 2 with a review of interference, models for product deformation, and the effect of compensation. Adoption of the Rubin Causal Model (RCM, Holland, 1986) is a significant and novel feature of our investigation in 3D printing, and it facilitates the study of interference. Section 3.1 summarizes the basic model and analysis for deformation of cylinders given by Huang et al. (2013). Our analyses are in Sections 3.2–3.5: we first describe an experimental design hypothesized to generate interference, then proceed with posterior predictive checks to demonstrate the existence of

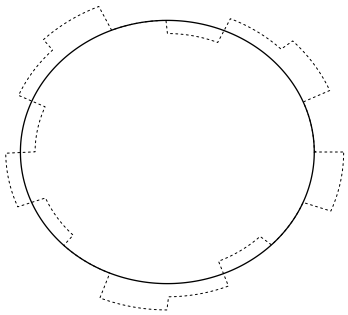

Fig 1: A discretized compensation plan (dashed-line) to the nominal boundary (solid line).

interference, and finally conclude with a model that captures interference. A statistically significant idea arising in Section 3.3 is that, in experiments explicitly making a distinction between *units of analysis* and *units of interpretation* (Cox and Donnelly, 2011, p. 18–19), the posterior distribution of model parameters, constructed using "benchmark" data, naturally leads to a simple assessment and inference for interference similar to that suggested by Sobel (2006) and Rosenbaum (2007). Analyses in Sections 3.4–3.5 demonstrate how discretized compensations complicate dimensional accuracy control along a product's boundary through the introduction of interference. This illustrates the fact that in complex manufacturing processes, a proper definition of experimental units and understanding of how units may interfere with each other are critical to quality control.

2. Potential Outcomes and Interference.

2.1. *Definition of Experimental Units and Potential Outcomes.* Suppose a product has intended shape ψ_0, and observed shape ψ under a 3D printing process. Deformation is informally described as the difference between ψ and ψ_0, where we can represent both either in the Cartesian coordinate system (x, y, z) or cylindrical coordinate system (r, θ, z). Cylindrical coordinates facilitate deformation modeling, and are used throughout.

For illustrative purposes, we define terms for two-dimensional products (notation for three dimensions follow immediately). Dimensional accuracy control requires an understanding of deformation in different regions of the

product that receive different amounts of compensation. We therefore define a finite number N points on the boundary of the product, corresponding to specific angles $\theta_1, \ldots, \theta_N$, as the experimental units. The desired boundary from the CAD model is defined by the function $r_0(\theta)$, denoting the nominal radius at angle θ. We consider only one (quantitative) treatment factor, compensation to the CAD, defined as a change in the nominal radius of the CAD by x_i units at θ_i for $i = 1, \ldots, N$. The potential radius for θ_i under the application of treatments $\mathbf{x} = (x_1, \ldots, x_N)$ to units $\theta_1, \ldots, \theta_N$ is a function of θ_i, $r_0(\cdot)$, and $\mathbf{x}$, denoted by $r(\theta_i, r_0(\cdot), \mathbf{x})$. The difference between the potential and nominal radius at θ_i defines deformation, and so we define

$$\Delta r(\theta_i, r_0(\cdot), \mathbf{x}) = r(\theta_i, r_0(\cdot), \mathbf{x}) - r_0(\theta_i) \tag{1}$$

as our *potential outcome* for θ_i. For now, potential outcomes are viewed as fixed numbers, with randomness introduced in Section 2.3 in our general model for the potential outcomes.

This definition of the potential outcome is convenient for visualizing shrinkage. For example, suppose the desired shape of the product is the solid line, and the manufactured product when $\mathbf{x} = \mathbf{0} = (0, \ldots, 0)$ is the dashed-line, in Figure 2(a). Plotting the deformation at each angle leads to a visualization amenable to analysis (Figure 2(b)). Orientation is fixed: we match the coordinate axes of the printed product with those of the CAD model.

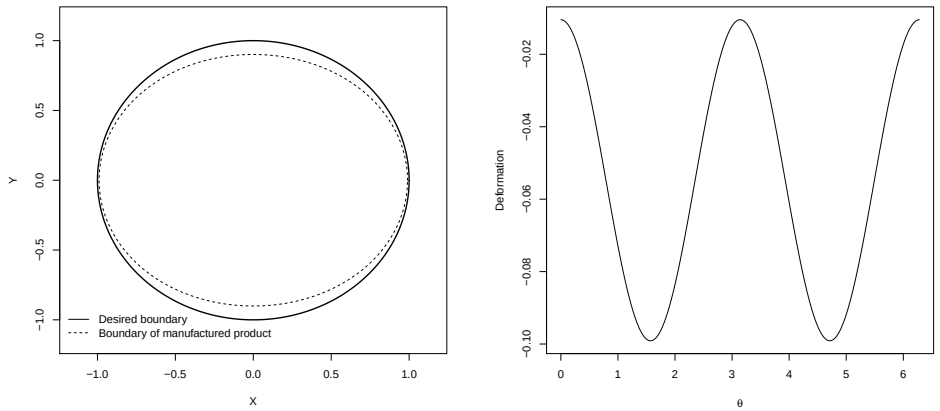

(a) (b)

Fig 2: **(a)**: Ideal shape (solid line) vs. the actual shape (dashed-line).
(b): Visualization of shrinkage.

2.2. *Interference.* A unit θ_i is said to be affected by interference if

$$\Delta r(\theta_i, r_0(\cdot), \mathbf{x}) \neq \Delta r(\theta_i, r_0(\cdot), \mathbf{x}')$$

for at least one pair of distinct treatment vectors $\mathbf{x}, \mathbf{x}' \in \mathbb{R}^N$ with $x_i = x_i'$ (Rubin, 1980). If there is no interference, then

$$\Delta r(\theta_i, r_0(\cdot), \mathbf{x}) = \Delta r(\theta_i, r_0(\cdot), x_i).$$

As the experimental units reside on a connected boundary, the deformation of one unit may depend on compensations assigned to its neighbors when the compensation plan is discretized. Perhaps less plausible, but equally serious, is the leakage of assigned compensations across units. These considerations explain the presence of the vector $\mathbf{x}$, containing treatment assignments for all units, in the potential outcome notation (1). Practically, accommodations made for interference should reduce bias in compensation plans for complex products, and improve dimensional accuracy control.

2.3. *General Deformation Model.* Our potential outcome model under treatment assignment $\mathbf{x} = \mathbf{0}$ is decomposed into three components:

$$\Delta r(\theta_i, r_0(\cdot), \mathbf{0}) = f_1(r_0(\cdot)) + f_2(\theta_i, r_0(\cdot), \mathbf{0}) + \epsilon_i. \tag{2}$$

Function $f_1(r_0(\cdot))$ represents average deformation of a given nominal shape $r_0(\cdot)$ independent of location θ_i, and $f_2(\theta_i, r_0(\cdot), \mathbf{0})$ is the additional location-dependent deformation, geometrically and physically related to the CAD model. We can also interpret $f_1(\cdot)$ as a lower order component and $f_2(\cdot, \cdot, \mathbf{0})$ as a higher order component of deformation. The ϵ_i are random variables representing high frequency components that add on to the main trend, with expectation $\mathbb{E}(\epsilon_i) = 0$ and $\mathrm{Var}(\epsilon_i) < \infty$ for all $i = 1, \ldots, N$. In all that follows, the ϵ_i are assumed to be independent and identically distributed. Correlation among the ϵ_i can also be addressed (Colosimo, Semeraro, and Pacella, 2008), and is the focus of our future work.

Figure 2 demonstrates model (2). In this example, $r_0(\theta) = r_0$, so $f_1(\cdot)$ is a function of r_0, and $f_2(0, r_0, \mathbf{0}) = f_2(2\pi, r_0, \mathbf{0})$. Decomposition of deformation into lower and higher order terms reduces (2) to

$$\Delta r(\theta_i, r_0, \mathbf{0}) = c_{r_0} + \sum_k \{a_{r_0,k} \cos(k\theta_i) + b_{r_0,k} \sin(k\theta_i)\} + \epsilon_i, \tag{3}$$

where $f_1(r_0) = c_{r_0}$, and $\{a_{r_0,k},\ b_{r_0,k}\}$ are coefficients of a Fourier series expansion of $f_2(\cdot, \cdot, \mathbf{0})$. The $\{a_{r_0,k},\ b_{r_0,k}\}$ terms with large k represent the product's surface roughness, which is not of primary interest.

2.4. *General Compensation and Interference Models.* Under the polar coordinate system, a compensation of x_i units at θ_i can be thought of as an extension of the product's radius by x_i units in that specific direction. Bearing this in mind, we now extend (2) to accommodate compensations.

Let $r(\theta_i, r_0(\cdot), (x_i, \ldots, x_i)) = r(\theta_i, r_0(\cdot), x_i)$ denote the potential radius for θ_i under application of x_i units of compensation to all points. Assuming that the dynamics of the manufacturing and deformation processes remain the same under compensation, we note that

$$r(\theta_i, r_0(\cdot), x_i) - \{r_0(\theta_i) + x_i\} = \Delta r(\theta_i, r_0(\cdot) + x_i, \mathbf{0}).$$

Consequently, the potential outcome for θ_i is

$$\begin{aligned} \Delta r(\theta_i, r_0(\cdot), x_i) &= r(\theta_i, r_0(\cdot), x_i) - r_0(\theta_i) \\ &= \Delta r(\theta_i, r_0(\cdot) + x_i, \mathbf{0}) + x_i. \end{aligned} \tag{4}$$

If x_i is small relative to $r_0(\theta_i)$, then the expectation of (4) can be approximated using the first and second terms of the Taylor expansion of $\mathbb{E}\{\Delta r(\theta_i, r_0(\cdot) + x_i, \mathbf{0})\}$ at $r_0(\theta_i)$:

$$\begin{aligned} \Delta r(\theta_i, r_0(\cdot), x_i) &\approx \mathbb{E}\{\Delta r(\theta_i, r_0(\cdot), \mathbf{0})\} \\ &\quad + (x_i - 0)\left[\frac{d}{dx}\mathbb{E}\{\Delta r(\theta_i, r_0(\cdot) + x, \mathbf{0})\}\right]_{x=0} + x_i + \epsilon_i \\ &= \Delta r(\theta_i, r_0(\cdot), \mathbf{0}) + \{1 + h(\theta_i, r_0(\cdot), \mathbf{0})\}x_i, \end{aligned} \tag{5}$$

where $h(\theta_i, r_0(\cdot), \mathbf{0}) = [d/dx\ \mathbb{E}\{\Delta r(\theta_i, r_0(\cdot) + x, \mathbf{0})\}]_{x=0}$. When a parametric model is specified for the potential outcomes, this Taylor expansion is performed conditional on the model parameters.

Interference can then be incorporated into (5) in a simple manner for a treatment assignment $\mathbf{x}$ having different units assigned different treatments. Specifically, although unit θ_i is assigned compensation x_i, we do not use only x_i to model the potential outcome for θ_i. Instead, we alter (5) to

$$\Delta r(\theta_i, r_0(\cdot), \mathbf{x}) \approx \Delta r(\theta_i, r_0(\cdot), \mathbf{0}) + \{1 + h(\theta_i, r_0(\cdot), \mathbf{0})\}g_i(\mathbf{x}), \tag{6}$$

where the *effective treatment* $g_i(\mathbf{x})$ is a function of x_i and assigned compensations for neighbors of θ_i (with the definition of neighboring units naturally dependent on the specific product), hence potentially a function of the entire vector $\mathbf{x}$. This change from x_i to $g_i(\mathbf{x})$ in (5) and (6) is based on the belief that the physical logic ultimately leading to (5) holds true on some level for general compensation plans. The simplest way to introduce interference is to allow the treatment effectively received by θ_i to depend on treatments

assigned to its neighboring units. As we shall see in the analysis of our experiment, this modification of the potential outcomes model effectively incorporates interference in a meaningful manner.

3. Experimental Design and Analysis for Interference.

3.1. *Compensation Model for Cylinders.* Huang et al. (2013) constructed four cylinders with $r_0 = 0.5, 1, 2$, and 3 inches, and used $N_{0.5} = 749, N_1 = 707, N_2 = 700$, and $N_3 = 721$ equally-spaced units from each, displayed in Figure 3(a). Based on the logic in Section 2.3, they fitted

$$\Delta r(\theta_i, r_0, \mathbf{0}) = x_0 + \alpha(r_0 + x_0)^a + \beta(r_0 + x_0)^b \cos(2\theta_i) + \epsilon_i \tag{7}$$

to the data, with $\epsilon_i \sim \mathrm{N}(0, \sigma^2)$ independently, and parameters α, β, a, b, x_0, and σ independent of r_0. Independent errors were used because the correlation of ϵ_i was not substantial enough to merit being modeled. They specified

$$a \sim \mathrm{N}(1, 2^2),\ b \sim \mathrm{N}(1, 1^2),\ \log(x_0) \sim \mathrm{N}(0, 1^2),$$

and placed flat priors on α, β, and $\log(\sigma)$, with all parameters independent *a priori*. Posterior draws of the parameters were obtained by Hamiltonian Monte Carlo (HMC, Duane, Kennedy, Pendleton, and Roweth, 1987), and are summarized in Table 1, with convergence diagnostics discussed in Appendix A. A simple comparison of the posterior predictive distribution of product deformation to the observed data (Figure 3(b)) demonstrates the good fit, and so we proceed with this specification and parameter inferences to design and analyze an experiment for interference.

TABLE 1
Summary of 1000 *posterior draws of parameters after a burn-in of* 500 *when no compensation is applied. This is drawn from Table* 5 *in (Huang et al., 2013).*

	Mean	SD	Median	95% Credible Interval	ESS
α	-1.34×10^{-2}	1.6×10^{-4}	-1.34×10^{-2}	$(-1.37, -1.31)\ \times 10^{-2}$	8198
β	5.7×10^{-3}	3.1×10^{-5}	5.71×10^{-3}	$(5.65, 5.8)\ \times 10^{-3}$	9522
a	8.61×10^{-1}	7.33×10^{-3}	8.61×10^{-1}	$(8.47, 8.75)\ \times 10^{-1}$	8223
b	1.13	5.46×10^{-3}	1.13	(1.12, 1.14)	9424
x_0	8.79×10^{-3}	1.5×10^{-4}	8.79×10^{-3}	$(8.5, 9.07)\ \times 10^{-3}$	8211
σ	8.7×10^{-4}	1.18×10^{-5}	8.7×10^{-4}	$(8.5, 8.9)\ \times 10^{-4}$	9384

Substituting $\Delta r(\theta_i, r_0, \mathbf{0})$ from (7) into the general model (4), we have

$$\Delta r(\theta_i, r_0, x_i) = x_0 + x_i + \alpha(r_0 + x_0 + x_i)^a + \beta(r_0 + x_0 + x_i)^b \cos(2\theta_i) + \epsilon_i. \tag{8}$$

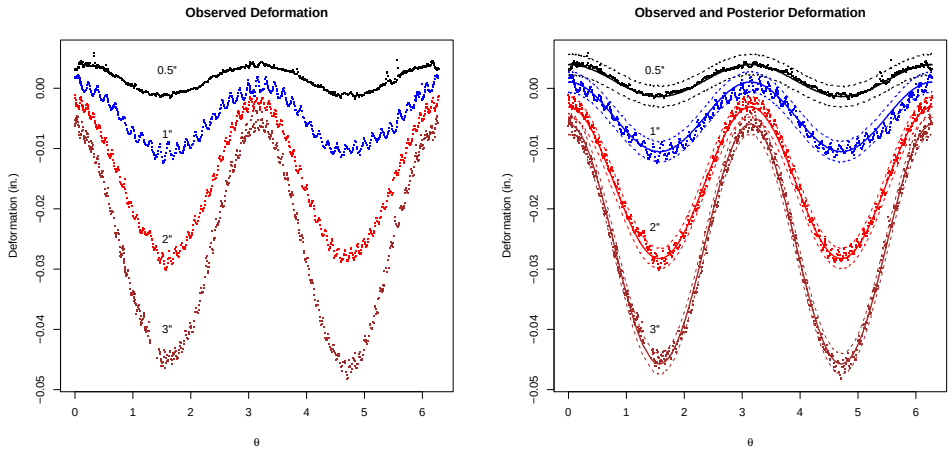

(a) (b)

Fig 3: **(a)**: Observed deformation for $r_0 = 0.5, 1, 2$, and 3 inches, when no compensation is applied. **(b)**: Comparison of observed data with posterior predictions. Bold solid lines denote posterior means, and dashed lines the 2.5% and 97.5% posterior quantiles for each angle. These are Figures 6 and 10 in (Huang et al., 2013).

The Taylor expansion at $r_0 + x_0$, as in (5), yields the model

$$\begin{aligned}\Delta r(\theta_i, r_0, x_i) &= x_0 + \alpha(r_0 + x_0)^a + \beta(r_0 + x_0)^b \cos(2\theta_i) \\ &\quad + \left\{1 + a\alpha(r_0 + x_0)^{a-1} + b\beta(r_0 + x_0)^{b-1} \cos(2\theta_i)\right\} x_i + \epsilon_i. \end{aligned} \tag{9}$$

We incorporate interference by changing x_i in (9) to $g_i(\mathbf{x})$, with the functional form of $g_i(\mathbf{x})$ derived by exploratory means in Section 3.3.

3.2. *Experimental Design for Interference.* Under a discretized compensation plan, the boundary of a product is divided into sections, with all points in one section assigned the same compensation. In the terminology of Cox and Donnelly (2011, p. 18–19), these sections constitute units of analysis, and individual angles are units of interpretation. We expect interference for angles near neighboring sections. Interference should be substantial for a large difference in neighboring compensations, and negligible otherwise.

This reasoning led to the following restricted Latin square design to study interference. We apply compensations to four cylinders of radius $0.5, 1, 2$, and 3 inches, with each cylinder divided into 16 equal-sized sections of $\pi/8$

radians. One unit of compensation is $0.004, 0.008, 0.016$, and 0.03 inch for each respective cylinder, and there are only four possible levels of compensation, $-1, 0, +1$, and $+2$ units. Two blocking factors are considered. The first is the quadrant, and the second is the "symmetry group" consisting of $\pi/8$-radian sections that are reflections about the coordinate axes from each other. Symmetric sections form a meaningful block: if compensation x is applied to all units, then we have from (9) that for $0 \leq \theta \leq \pi/2$,

$$\begin{aligned}\mathbb{E}\left\{\Delta r(\theta, r_0, x) \mid \alpha, \beta, a, b, x_0, \sigma\right\} &= \mathbb{E}\left\{\Delta r(\pi - \theta, r_0, x) \mid \alpha, \beta, a, b, x_0, \sigma\right\} \\ &= \mathbb{E}\left\{\Delta r(\pi + \theta, r_0, x) \mid \alpha, \beta, a, b, x_0, \sigma\right\} \\ &= \mathbb{E}\left\{\Delta r(2\pi - \theta, r_0, x) \mid \alpha, \beta, a, b, x_0, \sigma\right\},\end{aligned}$$

suggesting a need to control for this symmetry in the experiment. Finally, based on prior concerns about the possible severity of interference and resulting scope of inference from our model (5), treatments were randomly assigned to the 16 sections such that the absolute difference in assigned treatments between two sections cannot exceed two levels of compensation.

Our restricted Latin square design forms a discretized compensation plan that blocks on two factors suggested by the previous deformaton model, and remains model-robust to a certain extent. The chosen experimental designs are in Figure 4, and observed deformations are in Figure 5. There are $N_{0.5} = 6159, N_1 = 6022, N_2 = 6206$, and $N_3 = 6056$ equally-spaced angles considered for the four cylinders.

3.3. *Assessing the Structure of Interference.* Our first task is to assess which units have negligible interference in the experiment. To do so, we use the suggestions of Sobel (2006) and Rosenbaum (2007), who describe when interest exists in comparing a treatment assignment $\mathbf{x}$ to a baseline.

We have in Section 3.1 data on cylinders that receive no compensation (denoted by $\mathbf{D}_n$), and a model (7) that provides a good fit. Furthermore, we have a hypothesized model (9) for compensation when interference is negligible, which is a function of parameters in (7). If the manufacturing process is in control, posterior inferences based on $\mathbf{D}_n$ then yield, by (9), predictions for the experiment. In the absence of any other information, units in the experiment with observed outcomes deviating strongly from their predictions can be argued to have substantial interference. After all, if θ_i has negligible interference under assignment $\mathbf{x} = (x_1, \ldots, x_N)$, then

$$\Delta r(\theta_i, r_0, \mathbf{x}) = \Delta r(\theta_i, r_0, (x_i, \ldots, x_i)) = \Delta r(\theta_i, r_0, x_i).$$

This suggests the following procedure to assess interference:

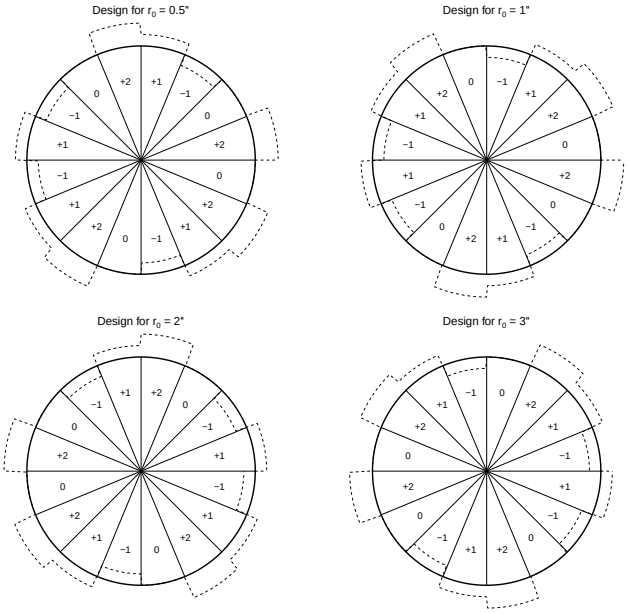

Fig 4: Experimental designs: dashed lines represent assigned compensations.

1. Calculate the posterior distribution of the parameters conditional on $\mathbf{D}_n$, denoted by $\pi(\alpha, \beta, a, b, x_0, \sigma \mid \mathbf{D}_n)$.
2. For every angle in the four cylinders, form the posterior predictive distribution of the potential outcome corresponding to the observed treatment assignment (Figure 4) using model (9) and $\pi(\alpha, \beta, a, b, x_0, \sigma \mid \mathbf{D}_n)$.
3. Compare the posterior predictive distributions to the observed deformations in the experiment.
    - If a unit's observed outcome falls within the 99% central posterior predictive interval and follows the posterior predictive mean trend, it is deemed to have negligible interference.
    - Otherwise, we conclude that the unit has substantial interference.

This procedure is similar to the construction of control charts (Box et al., 2009). When an observed outcome lies outside the 99% central posterior predictive interval, we suspect existence of a special cause. As the entire product is manufactured simultaneously, the only assignable cause is interference.

We implemented this procedure and observed that approximately $70\% - -80\%$ of units, primarily in the central regions of sections, have negligible interference (Appendix B). This is clearly seen with another graph that assesses effective treatments, which we proceed to describe.

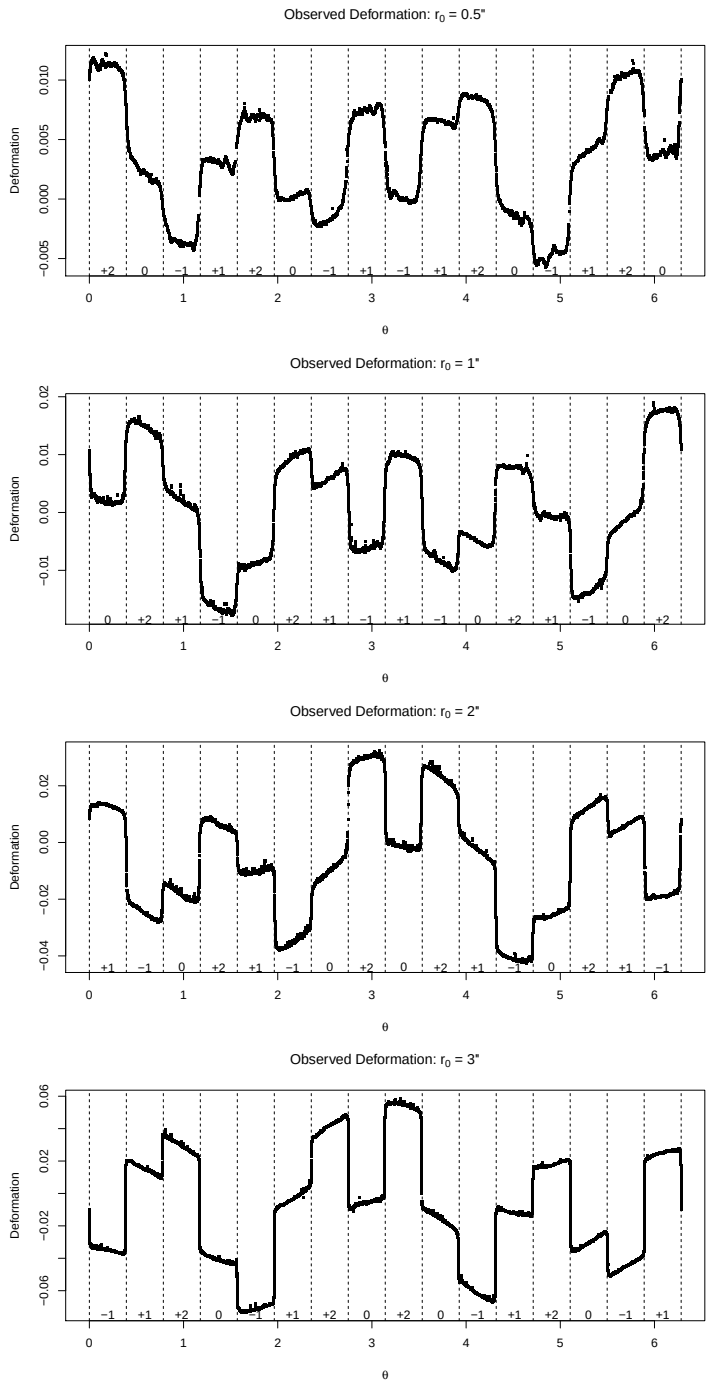

Fig 5: Observed deformations in the experiment. Dashed lines represent sections, and numbers at the bottom of each represent assigned compensations.

Taking expectations in (9), the treatment effectively received by θ_i is

$$\frac{\mathbb{E}\{\Delta r(\theta_i, r_0, \mathbf{x}) \mid \alpha, \beta, a, b, x_0, \sigma\} - x_0 - \alpha(r_0 + x_0)^a - \beta(r_0 + x_0)^b \cos(2\theta_i)}{1 + a\alpha(r_0 + x_0)^{a-1} + b\beta(r_0 + x_0)^{b-1}\cos(2\theta_i)}. \tag{10}$$

We use (10) to gauge $g_i(\mathbf{x})$ by plugging observed data from the experiment and posterior draws of the parameters based on $\mathbf{D}_n$ into this equation. These calculations, summarized in Figure 6, again suggest that central angles in each section have negligible interference: estimates of their effective treatments correspond to their assigned treatments. There is a slight discrepancy between assigned treatments and posterior predictive quantities for some central angles, but this is likely due to different parameter values for the two data sets. Of more importance is the observation that the effective treatment of a boundary angle θ_i is a weighted average of the treatment assigned to its section, $x_{i,M}$, and its nearest neighboring section, $x_{i,NM}$, with the weights a function of the distances (in radians) between θ_i and the midpoint angle of its section, $\theta_{i,M}$, and the midpoint angle of its nearest neighboring section, $\theta_{i,NM}$. All these observations correspond to the intuition that interference should be substantial near section boundaries.

3.4. *A Simple Interference Model.* We first alter (9) to

$$\begin{aligned}\Delta r(\theta_i, r_0, \mathbf{x}) &= x_0 + \alpha(r_0 + x_0)^a + \beta(r_0 + x_0)^b \cos(2\theta_i) \\ &\quad + \left\{1 + a\alpha(r_0 + x_0)^{a-1} + b\beta(r_0 + x_0)^{b-1}\cos(2\theta_i)\right\} g_i(\mathbf{x}) + \epsilon_i,\end{aligned} \tag{11}$$

where

$$\begin{aligned}g_i(\mathbf{x}) &= \{1 + \exp(-\lambda_{r_0}|\theta_i - \theta_{i,NM}| + \lambda_{r_0}|\theta_i - \theta_{i,M}|)\}^{-1} x_{i,M} \\ &\quad + \{1 + \exp(\lambda_{r_0}|\theta_i - \theta_{i,NM}| - \lambda_{r_0}|\theta_i - \theta_{i,M}|)\}^{-1} x_{i,NM},\end{aligned} \tag{12}$$

with $\theta_{i,M}, \theta_{i,NM}$ denoting midpoint angles for the $\pi/8$-radian sections containing and neighboring nearest to θ_i, respectively, and $x_{i,M}, x_{i,NM}$ treatments assigned to these sections. Effective treatment $g_i(\mathbf{x})$ is a weighted average of the unit's assigned treatment $x_i = x_{i,M}$ and the treatment $x_{i,NM}$ assigned to its nearest neighboring section. Although the form of the weights is chosen for computational convenience, we recognize that (12) belongs to a class of models agreeing with prior subject-matter knowledge that interference may be negligible if the implemented compensation is sufficiently "continuous", in the sense that the theoretical compensation plan is a continuous function of θ and the tolerance of the 3D printer is sufficiently fine so that discretization of compensation is negligible (Appendix C).

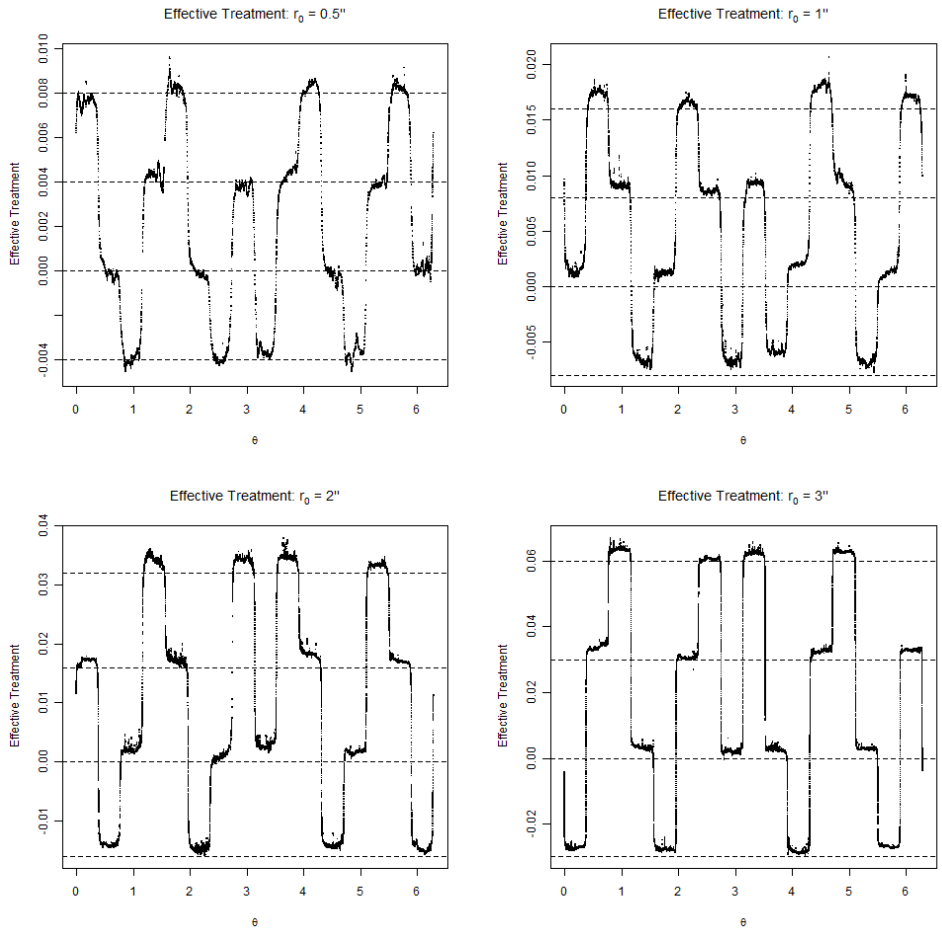

Fig 6: Gauging effective treatment $g_i(\mathbf{x})$ using (10). Four horizontal lines in each subfigure denote the possible compensations, and dots denote estimates of treatments that units effectively received in the experiment.

We fit the model in (11) and (12), having 10 total parameters, to the experiment data. The prior specification remains the same, with $\log(\lambda_{r_0}) \sim \mathrm{N}(0, 4^2)$ independently *a priori* for $r_0 = 0.5, 1, 2$, and 3 inches. A HMC algorithm was used to obtain 1000 draws from the joint posterior distribution after a burn-in of 500, and these are summarized in Table 2.

TABLE 2
Summary of posterior draws for simple interference model.

	Mean	SD	Median	95% Credible Interval	ESS
α	-1.06×10^{-2}	1.53×10^{-4}	-1.06×10^{-2}	$(-1.09, -1.03) \times 10^{-2}$	8078
β	5.79×10^{-3}	3.69×10^{-5}	5.79×10^{-3}	$(5.72, 5.86) \times 10^{-3}$	8237
a	9.5×10^{-1}	9.46×10^{-3}	9.5×10^{-1}	$(9.31, 9.69) \times 10^{-1}$	8150
b	1.12	6.64×10^{-3}	1.12	(1.0, 1.13)	8504
x_0	7.1×10^{-3}	1.43×10^{-4}	7.1×10^{-3}	$(6.82, 7.39) \times 10^{-3}$	8404
σ	3.14×10^{-3}	1.36×10^{-5}	3.14×10^{-3}	$(3.11, 3.17) \times 10^{-3}$	8924
$\lambda_{0.5}$	32.66	2.05	32.62	(28.69, 36.76)	8686
λ_1	48.24	2	48.12	(44.5, 52.6)	8666
λ_2	76.83	1.78	76.78	(73.42, 80.44)	8770
λ_3	86.08	0.83	86.06	(84.49, 87.68)	8385

This model provides a good fit for the 0.5 and 1 inch cylinders, but not the others. As an example, in Figure 7(a) the posterior mean trend does not correctly capture the observed transition across sections for the 3 inch cylinder. The problem appears to reside in (12). This specification implies that effective treatments of units $\theta_i = k\pi/8$ for $k \in \mathbb{Z}_{>0}$ are equal-weighted averages of compensations applied to units $k\pi/8 \pm \pi/16$. To assess the validity of this implication, we use the posterior distribution of the parameters to calculate, for each θ_i, the inferred effective treatment in (10). An example of these calculations, Figure 7(b), shows that the inferred effective treatment for $\theta_i = \pi$ is nearly 0.06 inch, the compensation applied to its neighboring section. Thus, specification (12) is invalidated by the experiment.

Another posterior predictive check helps clarify the problem. From (12),

$$g_i(\mathbf{x}) = w_i x_{i,M} + (1 - w_i) x_{i,NM},$$

and so

$$w_i = \frac{g_i(\mathbf{x}) - x_{i,NM}}{x_{i,M} - x_{i,NM}}, \tag{13}$$

which is well-defined because $x_{i,M} \neq x_{i,NM}$ in this experiment. Plugging in the inferred effective treatments, calculated from (10), into (13), we then diagnose how to modify (12) to better model interference in the experiment.

This calculation was made for all cylinders, and the results for $r_0 = 3$ inches are summarized in Figure 8 as an example. Rows in this figure show

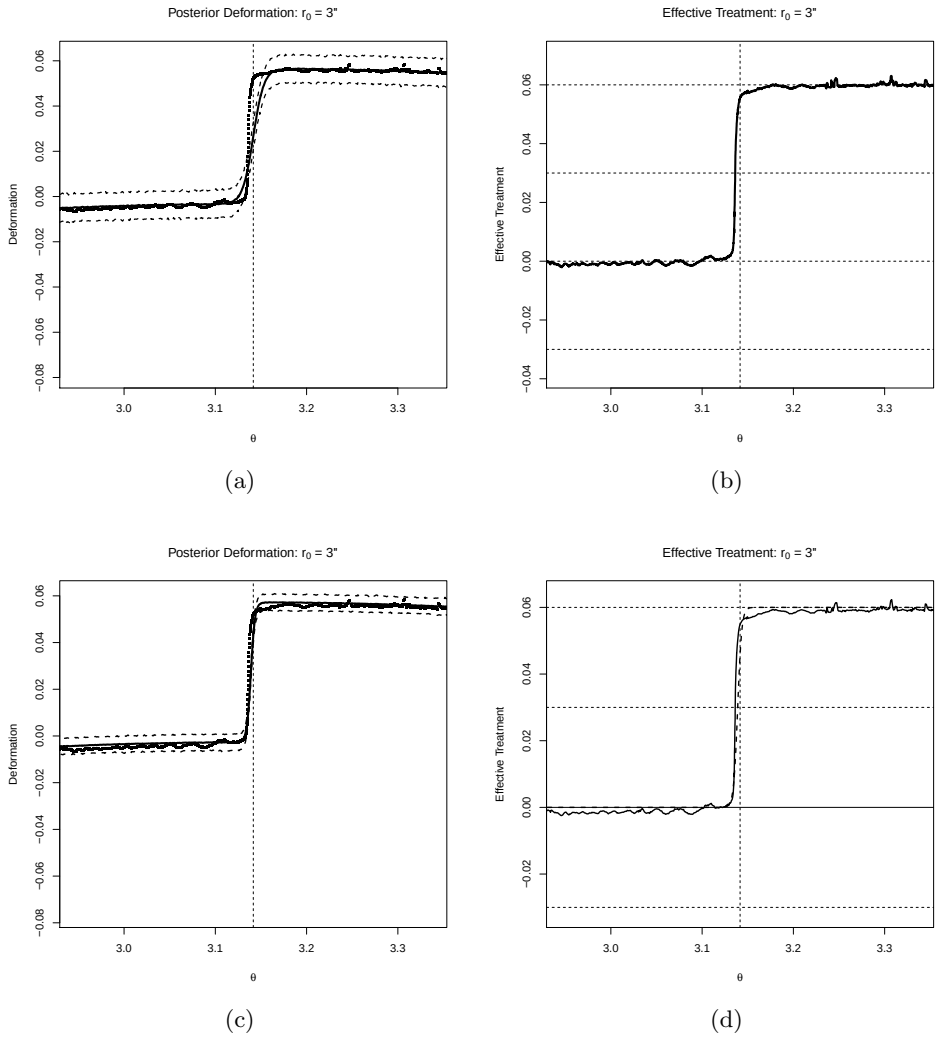

Fig 7: **(a)**: An example of the type of erroneous predictions made by model (11), (12) for the 3 inch cylinder. The vertical line is drawn at $\theta = \pi$, marking the boundary between two sections. Units to the left of this line were given 0 compensation, and units to the right were given +2 compensation. The posterior mean trend is represented by the solid line, and posterior quantiles are represented by dashed lines. Observed data are denoted by dots.
(b): Corresponding inferred effective treatment for $15\pi/16 \leq \theta \leq 17\pi/16$.
(c): Refined posterior predictions for $r_0 = 3''$, $15\pi/16 \leq \theta \leq 17\pi/16$.
(d): Comparing inferred effective treatments (solid line) with refined effective treatment model (dashed-line) for the 3 inch cylinder.

the weights for each quadrant, and we focus on their behavior in neighborhoods of integral multiples of $\pi/8$. Neither the decay in the weights (represented by λ_{r_0} in (12)) nor the weight for integral multiples of $\pi/8$ remain constant across sections. In fact, these figures suggest that λ_{r_0} is a function of $\theta_{i,M}, \theta_{i,NM}$, and that a location term is required.

3.5. *A Refined Interference Model.* Our refined effective treatment model is of the same functional form as (12), with λ_{r_0} replaced by $\lambda_{r_0}(\theta_{i,M}, \theta_{i,NM})$, and $|\theta_i - \theta_{i,M}|, |\theta_i - \theta_{i,NM}|$ replaced by $|\theta_i - \theta_{i,M} - \delta_{r_0}(\theta_{i,M}, \theta_{i,NM})|, |\theta_i - \theta_{i,NM} - \delta_{r_0}(\theta_{i,M}, \theta_{i,NM})|$, respectively. Here, $\delta_{r_0}(\theta_{i,M}, \theta_{i,NM})$ represent location shifts across sections suggested by our posterior predictive checks.

Our specific model is

$$\delta_{r_0}(\theta_{i,M}, \theta_{i,NM}) = \delta_{r_0,0} + \sum_{k=1}^{3} \left\{ \delta^c_{r_0,k} \cos(k\theta_{i,B}) + \delta^s_{r_0,k} \sin(k\theta_{i,B}) \right\}, \tag{14}$$

$$\lambda_{r_0}(\theta_{i,M}, \theta_{i,NM}) = \mathbb{I}(|x_{i,M} - x_{i,NM}| = 1)\lambda_{r_0,1} + \mathbb{I}(|x_{i,M} - x_{i,NM}| = 2)\lambda_{r_0,2}, \tag{15}$$

where $\theta_{i,B} = (\theta_{i,M} + \theta_{i,NM})/2$ and $|x_{i,M} - x_{i,NM}|$ is measured in absolute units of compensation here. From Figure 8 and the fact that

$$\delta_{r_0}(\theta_{i,M}, \theta_{i,NM}) = \delta_{r_0}(\theta_{i,M} + 2\pi, \theta_{i,NM} + 2\pi),$$

location shifts should be modeled using harmonic functions.

This model provides a better fit. Comparing Figure 7(c), which displays posterior predictions from the refined model (based on one chain of posterior draws using a standard random walk Metropolis algorithm), with the previous model's predictions in Figure 7(a), we immediately see that the refined model better captures the posterior mean trend. Similar improvements exist for the other sections and cylinders. We also compare the original inferred effective treatments obtained from (10) with the refined model in Figure 7(d) and see that the new model better captures interference.

3.6. *Summary of the Experimental Design and Analysis.* Three key ingredients relating to the data, model, and experimental design have made our series of analyses possible. First is the availability of benchmark data, e.g., every unit on the cylinder receiving zero compensation. Second is the potential outcomes model (9) for the effect of compensation, defined in terms of a fixed number of parameters that do not depend on the vector of treatment assignments $\mathbf{x}$. These two enable calculation of the posterior predictive

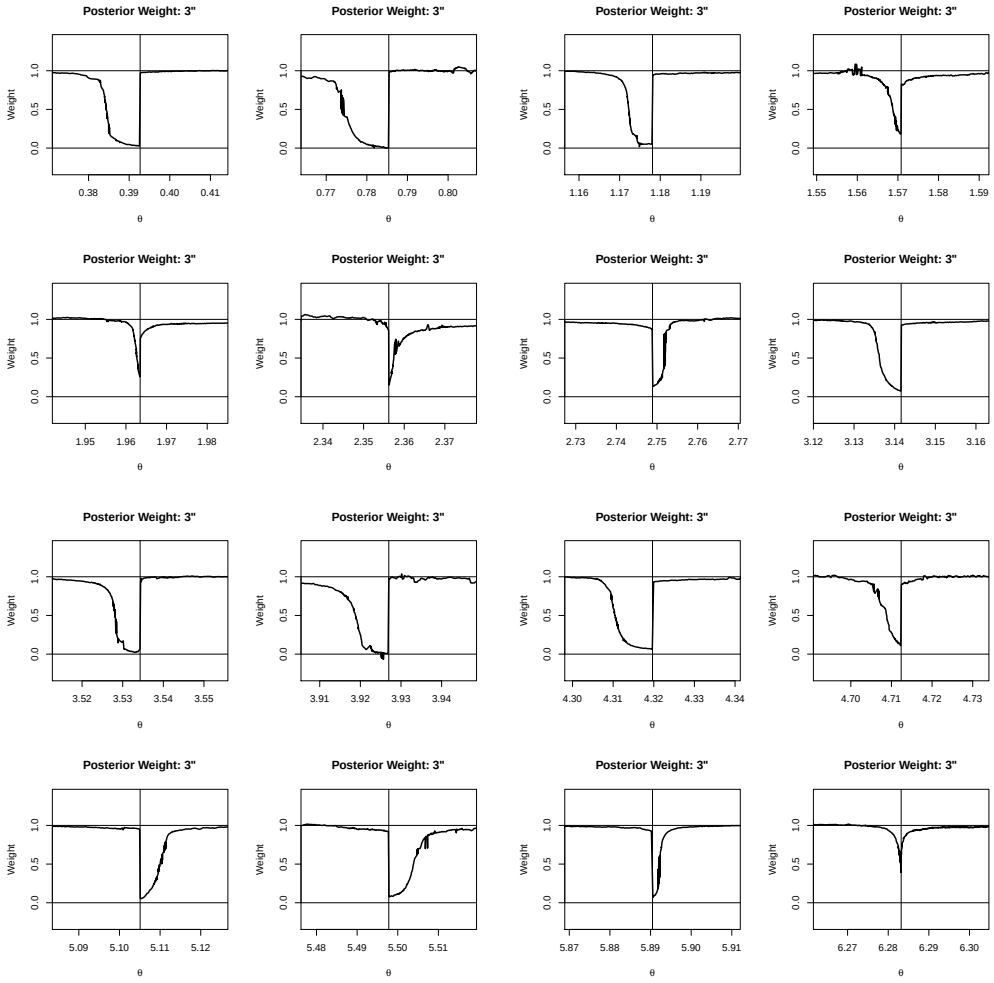

Fig 8: Inferring weights in the interference model for the $r_0 = 3$ inch cylinder, using effective treatments calculated from equation (10) based on the posterior distribution of parameters from Section 3.4. Vertical lines are drawn at $\theta = k\pi/8$ for $k = 1, \ldots, 16$.

distribution of potential outcomes under the assumption of negligible interference. The final ingredient is the explicit distinction between units of analysis and units of interpretation in our design, which provides the means to assess and model interference in the experiment. Comparing observed outcomes from the experiment to posterior predictions allows one to infer the structure of interference, which can be validated by further experimentation.

These considerations suggest that our methodology can be generalized and applied to other experimental situations with units residing on connected surfaces. In fact, the three ingredients above appear to be relevant and useful across a wide variety of disciplines. For example, in agricultural experiments for the effects of fertilizers on crop yield, we can use data from uniformity trials and models for crop yield when all plots in a field are given the same fertilizer to assess interference when different plots are assigned different fertilizers. As in our experiment, the plots reside on a connected surface, namely the field, and we expect interference to be substantial along the boundaries of the plots. In general, when experimenting with units on a connected surface, a principled and step-by-step analysis using the three ingredients above, as illustrated in this paper, can ultimately shed more light on the substantive question of interest.

4. Conclusion: Ignoring Interference Inhibits Improvements. To construct 3D printed products satisfying manufacturing demands on dimensional accuracy, it is important to address the problem of interference in a principled manner. Huang et al. (2013) recognized that continuous compensation plans implemented on printers with a sufficiently fine tolerance can effectively control a product's printed dimensions without inducing additional complications through interference. Their models for product deformation motivated our experiment that introduces interference through the application of a discretized compensation plan to the boundary of a cylinder. Combining this experiment's data with inferences based on data for which every unit received no compensation led to an assessment of interference in terms of how units' effective treatments differed from that physically assigned. Further analyses effectively modeled interference in the experiment.

It is important to note that the refined interference model's location and scale terms (14), (15) are a function of the compensation plan. For example, reflecting the assigned compensations across the y axis would accordingly change the location shifts. The implication of this and all our previous observations for manufacturing is that severely discretized compensation plans introduce interference, and if this fact is ignored, then dimensional accuracy control for 3D printed products will be hindered, especially for geometrically

complex products relevant in real-life manufacturing.

It is worthwhile to note that there is an interesting connection between interference modeling and the classic robust design approach (Taguchi, 1987) for dimensional accuracy control in 3D printing. As pointed out by several authors, e.g., Wu and Hamada (2009, Ch. 11) and Dasgupta and Wu (2006), response function modeling is a useful step in any robust design problem, when the response is modeled as a function of control and noise factors, and a suitable performance measure (e.g., the signal-to-noise ratio) is derived from the fitted response function. The principle of robust design can successfully be applied only if the response model contains interaction terms between the control factors and the noise factors. In our current context, as before, let x_i denote the compensation applied to the ith unit, and $\mathbf{x}_i^-$ the compensations applied to all other units. Then obtaining an optimal or "robust" compensation entails the following two steps: (i) expressing the deformation as a function $\Delta r(\theta_i, r_0(\cdot), x_i, \mathbf{x}_i^-)$, and (ii) choosing $\mathbf{x}$ such that a performance measure of unit-level deformation is minimized. Our focus on understanding interference between units can also be viewed as identifying significant interactions between x_i and $\mathbf{x}_i^-$ and fitting an appropriate response function model, which is nothing but response function modeling in the robust design context. The question of robustness only arises if such interactions exist.

Many research challenges and opportunities for both statistics and additive manufacturing remain to be addressed. Perhaps the most important is experimental design in the presence of interference. For example, when focus is on construction of specific classes of products (e.g., complicated gear structures), optimum designs can lead to precise estimates of model parameters, hence improved compensation plans and control of deformation. An important and subtle statistical issue that then arises is how the structure of interference changes as a function of the compensation plan derived from the experimental design. Instead of being a weighted average of the treatment applied to its section and nearest neighboring section, the derived compensation plan may cause a unit's effective treatment to be a weighted average of treatments applied to other sections as well, with weights depending on the absolute difference in applied compensations. Knowledge of the relationship between compensation plans derived from specific experimental designs and interference is necessary to improve dimensional accuracy control in general, and therefore is an important issue to address for 3D printing.

APPENDIX A: MCMC CONVERGENCE DIAGNOSTICS

Convergence of our MCMC algorithms was gauged by analysis of ACF and trace plots, and effective sample size (ESS) and Gelman and Rubin (GR, 1992) statistics, which were calculated using 10 independent chains of 1000 draws after a burn-in of 500. In Sections 3.1 and 3.4, the ESS were all above 8000 (the maximum is 10000), and the GR statistics were all 1.

APPENDIX B: ASSESSING INTERFERENCE

The results of the first procedure described in Section 3.3 are displayed in Figure 9: bold lines represent posterior means, dashed lines quantiles forming the 99% central posterior intervals, and dots the observed outcomes in the experiment, with separate figures for each nominal radius and compensation. For example, the graph in the first row and column of Figure 9 contains the observed data for angles in the 0.5 inch radius cylinder that received -1 compensation. This figure also contains the posterior predictive mean and 99% intervals for all angles under the assumption that -1 compensation was applied uniformly to the cylinder. Although only four sections of the cylinder received this compensation in the experiment, forming this distribution makes the posterior predictive mean trend transparent, and so helps identify when a unit's observed outcome deviates strongly from its prediction.

APPENDIX C: NOTE ON A CLASS OF INTERFERENCE MODELS

Compensation is applied in practice by discretizing the plan at a finite number of points, according to some tolerance specified by the size (in radians) for each section, or alternatively the maximum value of $|\theta_{i,M} - \theta_{i,NM}|$.

Suppose compensation plan $x(\theta)$ is a continuous function of θ, and define

$$w_i = \frac{h(|\theta_i - \theta_{i,M}|)}{h(|\theta_i - \theta_{i,M}|) + h(|\theta_i - \theta_{i,NM}|)},$$

with $h : \mathbb{R} \to \mathbb{R}_{>0}$ a monotonically decreasing continuous function, and

$$g_i(\mathbf{x}) = w_i x_{i,M} + (1 - w_i) x_{i,NM}.$$

Then for the cylinder product considered in our experiment, $g_i(\mathbf{x}) \to x_i$ as $|\theta_{i,M} - \theta_{i,NM}| \to 0$. To show this, we first recognize that $|x_{i,M} - x_{i,NM}| \to 0$ as $|\theta_{i,M} - \theta_{i,NM}| \to 0$. Therefore, as

$$0 \leq |\theta_i - \theta_{i,NM}| - |\theta_i - \theta_{i,M}| \leq |\theta_{i,M} - \theta_{i,NM}|,$$

$g_i(\mathbf{x}) \to x_i$ as $|\theta_{i,M} - \theta_{i,NM}| \to 0$.

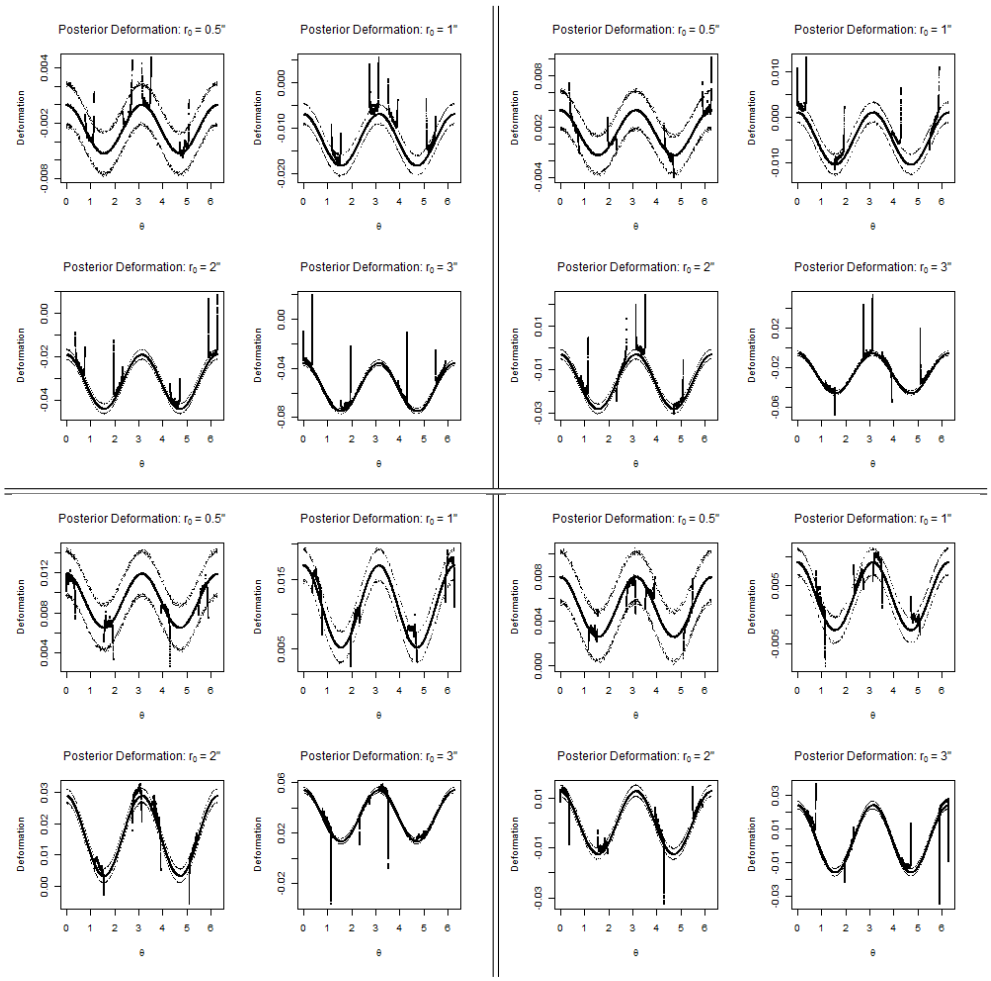

Fig 9: Assessing interference in the experiment based on posterior inferences drawn from the no-compensation data. Clockwise from top left: predictions for units that received $-1, 0, +1$, and $+2$ compensation.

ACKNOWLEDGEMENTS

We are grateful to Xiao-Li Meng, Joseph Blitzstein, David Watson, Matthew Plumlee, and an Associate Editor for their valuable comments, which improved this paper.

REFERENCES

Box, G., A. Luceño, and M. Paniagua-Quiñones (2009). *Statistical Control by Monitoring and Adjustment* (2 ed.). Wiley.

Campbell, T., C. Williams, O. Ivanova, and B. Garrett (2011). *Could 3D Printing Change the World? Technologies, Potential, and Implications of Additive Manufacturing*. Washington, DC: Atlantic Council.

Colosimo, B. M., Q. Semeraro, and M. Pacella (2008). Statistical process control for geometric specifications: on the monitoring of roundness profiles. *Journal of Quality Technology 40*(1), 1–18.

Cox, D. and C. Donnelly (2011). *Principles of Applied Statistics* (1 ed.). Cambridge University Press.

Dasgupta, T. and C. F. J. Wu (2006). Robust parameter design with feedback control. *Technometrics 48*(3), 349–360.

Duane, S., A. Kennedy, B. J. Pendleton, and D. Roweth (1987, September). Hybrid Monte Carlo. *Physics Letters B 195*(2), 216–222.

Gelman, A. and D. Rubin (1992). Inference from iterative simulation using multiple sequences. *Statistical Science 7*(4), 457–472.

Gibson, I., D. Rosen, and B. Stucker (2009). *Additive Manufacturing Technologies: Rapid Prototyping to Direct Digital Manufacturing*. Springer Verlag.

Hilton, P. and P. Jacobs (2000). *Rapid Tooling: Technologies and Industrial Applications*. CRC.

Holland, P. W. (1986). Statistics and causal inference. *Journal of the American Statistical Association 81*(396), 945–960.

Huang, Q., J. Zhang, A. Sabbaghi, and T. Dasgupta (2013). Optimal offline compensation of shape shrinkage for 3D printing processes. *IIE Transactions* (accepted).

Melchels, F., J. Feijen, and D. Grijpma (2010). A review on stereolithography and its applications in biomedical engineering. *Biomaterials 31*(24), 6121–6130.

Rosenbaum, P. (2007). Interference between units in randomized experiments. *Journal of the American Statistical Association 102*(477), 192–200.

Rubin, D. (1980). Comment on "Randomization analysis of experimental data: the Fisher randomization test," by D. Basu. *Journal of the American Statistical Association 75*, 591–593.

Sobel, M. (2006). What do randomized studies of housing mobility demonstrate?: causal inference in the face of interference. *Journal of the American Statistical Association 101*(476), 1396–1407.

Taguchi, G. (1987). *The System of Experimental Design: Engineering Methods to Optimize Quality and Minimize Costs* (1 ed.). Quality Resources.

Tong, K., S. Joshi, and E. Lehtihet (2008). Error compensation for fused deposition modeling (fdm) machine by correcting slice files. *Rapid Prototyping Journal 14*(1), 4–14.

Tong, K., E. Lehtihet, and S. Joshi (2003). Parametric error modeling and software error compensation for rapid prototyping. *Rapid Prototyping Journal 9*(5), 301–313.

Wang, W., C. Cheah, J. Fuh, and L. Lu (1996). Influence of process parameters on stereolithography part shrinkage. *Materials & Design 17*(4), 205–213.

Wu, C. F. J. and M. S. Hamada (2009). *Experiments: Planning, Analysis, and Optimization* (2 ed.). Wiley Series in Probability and Statistics. Wiley.

Arman Sabbaghi
Tirthankar Dasgupta
Department of Statistics
1 Oxford Street, 7th Fl.
Cambridge, MA 02138
E-mail: sabbaghi@fas.harvard.edu
E-mail: dasgupta@stat.harvard.edu

Qiang Huang
Jizhe Zhang
Daniel J. Epstein Department of
Industrial and Systems Engineering
3715 McClintock Avenue
Los Angeles, CA 90089
E-mail: qiang.huang@usc.edu
E-mail: jizhezha@usc.edu